$ZnMn_2O_4$-Based Anode Materials for Advanced Supercapacitor Batteries: A Study on the Impact of Co, Ni, and Cu partially substitution on Electrochemical Performance

S Bixa, MLA Letswalo, and B Sondezi

Department of Physics, University of Johannesburg, 55 Beit St, Doornfontein, Johannesburg, 2028, South Africa.

E-mail: letswalom@uj.ac.za and bmsondezi@uj.ac.za

Abstract.

A series of $ZnMn_2O_4$ samples partially doped with Co, Ni, and Cu 1 wt% were synthesized via combustion method and evaluated for improved electrochemical performance. The synthesized powders were thoroughly characterized using XRD, FE-SEM, and electrochemical techniques (GCD, CV, and EIS) to evaluate their performance as anode materials for supercapacitor batteries. The XRD results revealed that the incorporation of Co, Ni, and Cu metals did not alter the crystal structure of $ZnMn_2O_4$. However, the FE-SEM data showed that the addition of these metals modified the particle shapes and sizes. The optimum particle size of the doped $ZnMn_2O_4$ was found to be in the range of 36.33 - 41.29 nm. Notably, the Co-doped $ZnMn_2O_4$ exhibited superior performance in battery cycling tests (GCD), demonstrating exceptional discharge capacity, cycling stability, and rate capability compared to other metal oxides with 686.88 Fg^{-1} specific capacitance. Furthermore, the Co-doped $ZnMn_2O_4$ showed great performance in (CV) at a low scan rate of 5 mVs^{-1} with 48.85 Fg^{-1} specific capacitance, and it also displayed a pseudocapacitance behavior. EIS demonstrated a great performance for Cu-doped $ZnMn_2O_4$ having lowest resistance due to smallest-semicircle. Furthermore, its steeper vertical line indicates that it has good potential for use as an anode material in supercapacitor applications.

1 Introduction

The burning of fossil fuels releases gas emissions, which have serious consequences and lead to ecological concerns and global warming. A carbon-free society built on sustainable and renewable energy resources could solve these problems. The need to meet environmental and energy demands has prompted humanity to reevaluate its efforts in energy revitalization. The development of larger and better-capacity energy storage systems (ESSs) has made this need possible. The energy storage sources, like supercapacitors and lithium-ion batteries, might be considered beneficial in such endeavors [1]

$ZnMn_2O_4$ (ZMO), a spinel structured material, with a general formula of AMn_2O_4, exhibits unique properties that work well in energy storage batteries. ZMO, a spinel structured metal oxide, has been highly researched for its applications in supercapacitor batteries due to its environmental friendliness, effectiveness, and high electrical conductivity. The structural stability during charge and discharge for these materials processes is vital for sustaining the lifespan of these energy storage device systems and performance [2]. Xueling Zhu et al. [3] synthesized Co-doped $ZnMn_2O_4$ hallow nanospheres, using the hydrothermal method at lower concentrations. They observed that incorporating Co into $ZnMn_2O_4$ material could enhance its electrochemical behavior, thereby revealing the great value of specific capacitance, of 296 Fg^{-1} at 0.25 Ag^{-1} [3]. Hasan M et al. [4] used the sol-gel method to study Ni-doped $ZnMn_2O_4$ for its porous architectural structural at varied concentrations. They found the material to possess exceptional capacitive behavior, with a value of 8.49 Fg^{-1}, thereby proving the material to be a supercapacitor. Salma Aman et al. [5] used the hydrothermal method to study Cu-substituted $ZnMn_2O_4$/rGO

spinel nanosized composite as an electrode for OER (Oxygen evaluation reaction). Their results confirmed an enhanced electrocatalytic efficiency for a material of a hybrid nature [5].

In this study, we will study the ZMO material using the combustion synthesis method at varied concentrations of (1 wt%) to check its stability, cycle life, and power density characteristics. Electrochemical properties such as cyclic voltammetry (CV), galvanic charge and discharge (GCD), and electrochemical impedance spectroscopy (EIS) are among these characterizations, including X-ray diffraction (XRD), scanning electron microscopy (SEM), energy dispersive X-ray spectroscopy (EDS).

2 Experimental details

2.1 Synthesis of $ZnMn_2O_4$

ZMO doped Co, Ni, and Cu (x = 0, and 1 wt%) were synthesized through the combustion method. The starting materials in this study are $Zn(NO_3)_2.6H_2O$ 99%, $MnCl_2.4H_2O$ 99%, (CH_4N_2O) 99%, $Cu(No_3)_2.3H_2O$ 99% which were obtained from India SRL laboratory. A volume of 40 ml of de-ionized water was poured into a 250 ml beaker and stirred for about 10 minutes, then 3.868 g of zinc nitrate was added to the beaker until it was dissolved. A mass of 5.148 g of manganese chloride was then added to the solution and stirred for about 10 minutes until it was dissolved and the color of the solution changed to pink. An additional mass of 15.626 g of urea was also added to the solution and stirred until it dissolved. After that, a few drops of ammonia solution were added to the solution until a pH of 9 was reached. The solution was further stirred for 4 hours and finally formed a brownish color. The solution was taken to the furnace and heated at 500˚C for 1 hour. After cooling, it was ground and annealed at 550˚C for 2 hours and 30 minutes. The doped samples where the ratios of Co, Ni, and Cu (0.0376, 0.1134, and 0.190 g) were added to substitute Zn $(NO_3)_2.6H_2O$ partially.

The electrochemical performance of the supercapacitors was investigated by using Biologic EC-lab V11.50 SP 300 potentiostat with 3 electrodes, working (active material), Counter (Platinum), and reference (Ag/Agcl) electrode in 2 M KOH electrolytes for CV, GCD, and EIS. The three-electrode system was constructed by the ratio of 80 wt%:10 wt%:10 wt%. First, the synthesized powder ZMO sample (80 wt%), with carbon black (10 wt%), and a binder, polyvinylidene fluoride binder (PVDF, 10 wt%) were solvent N-methyl-2-pyrrolidone (NMP) was used to form a solution. The resulting solution was coated onto a nickel foam substrate using a brush. After that, the sample was dried in a vacuum oven at 80 ˚C for half a day, and the composite-coated substrate was cut into pieces of ~10 mm diameter. The mass of active material that was loaded was about 2 mg.

3. Results and Discussion

3.1 X-ray diffraction analysis

Figure 1(a) shows the XRD pattern for the ZMO material prepared by the combustion synthesis method. The spinel structure of Co, Ni, and Cu doped material with concentrations of (1 wt%) are illustrated by the pattern with the 2θ range of 10-80º. The XRD diffraction pattern reveals major peaks corresponding with the planes at (101), (112), (200), (103), (211), (202), (004), (220), (204), (105), (312), (303), (321), (224) along with several minor diffraction peaks [6]. The XRD diffraction pattern corresponds to that of a tetragonal spinel structure of ZMO, with unit cell lattice parameters of $a = b$ 5.71937Å, c = 9.28138Å, and V = 303.621Å^3 and a space group of 141/amd. This is consistent with the standard references JCPDS file no:01-077-0470 [6].

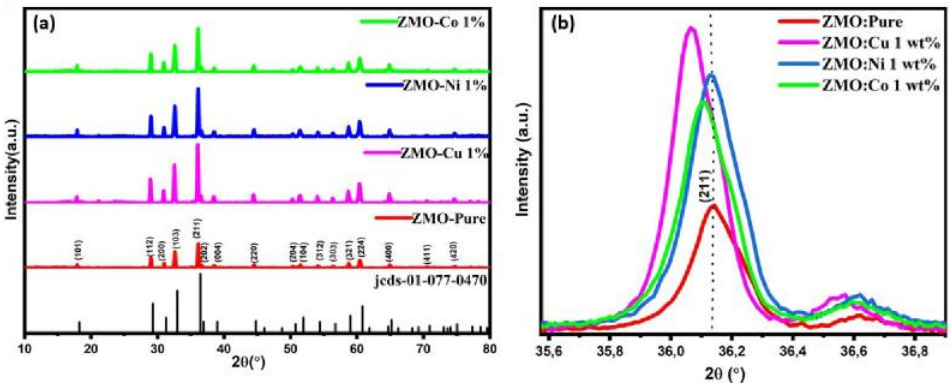

Figure 1: (a) XRD of Co, Ni, and Cu -doped $ZnMn_2O_4$ with concentration of (x = 0, 1 wt%), (b) enlarged pattern peak of (211) at various concentrations.

Figure 1(b) shows an enlarged diffraction pattern of XRD in the selected 2θ range of 35.6˚ to 37.02˚ corresponding to the (211) plane. As the concentration of Cu 1 wt% is being introduced to the material (ZMO), the crystal lattice contracts, resulting in an increase in the intensity of the diffraction peaks. Differences in the ionic radii of the dopants Co, Ni and Cu having (0.0745 nm), (0.069 nm) and (0.074 nm) respectively, cause a shift. while Ni increased in intensity. The improved intensity may be attributed to enhanced crystallinity in the particle arrangements, a shift to the left would suggest less clustering and lower strain, while a change to the right might suggest more clustering and higher strain [7].

3.2 Surface morphology (SEM) and elemental composition

The morphology of Co, Ni, and Cu doped ZMO material was investigated by using scanning electron microscopy (SEM), and Energy-dispersive X-ray spectroscopy (EDS) was used for the element composition. Figure 2(a-d) illustrates the SEM micrographs and EDS characterization of the material [8]. Figure 2(a) shows the diamond-like shape with irregular nanoparticles exhibiting aggregation. As the Cu concentration of 1 wt% is added to the host, as illustrated in Figure 2(b), the existence of a catalyst, nanoparticle, appears more than in the host, and the particle size is larger due to the ionic radius of 0.074 nm. Figure 2(c) illustrates ZMO-Ni the number of catalyst-type nanoparticles, also increases, indicating that the material might improve the electrochemical properties. The size is smaller due to the lower ionic radius of 0.069 nm. As the Co is incorporated within the host, as shown in Figure 2(d), the number of catalyst-like nanoparticles increases with diamond-like shape structure. Figure 2(a) displays the doped elemental composition of Cu doped ZMO, having Zn, Mn, O, Cu and Cl present due to the manganese chloride salt due to synthesis. Figure (b), (c), and (d) exhibit the EDS of the doped Cu, Ni, and Co elements with presence of Cl coming from the synthesis. The Ir element was used as a coating on the non-conducting material to ensure the accuracy of the obtained results [8-9].

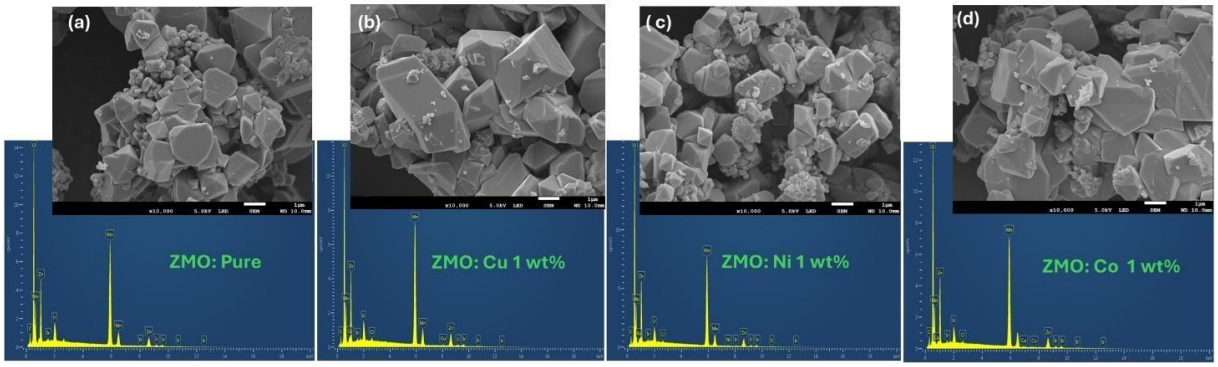

Figure 2: SEM Morphology image and EDS of Co, Ni, and Cu-doped $ZnMn_2O_4$ (a) ZMO, (b) ZMO: Cu 1 wt%, (c) ZMO: Ni 1 wt%, and (d) ZMO: Co 1 wt%

3.3 Electrochemical performance

3.3.1 Cyclic voltammetry (CV)

The electrochemical performance of the prepared material was measured in (CV) under a potential window range of 0-0.6 V at a scan rate of 5 to 100 mVs^{-1} in the presence of 2 M potassium hydroxide (KOH) electrolyte solution in a three-electrode system [4]. All the CV curves show a common shape of a pseudocapacitance nature, as shown in Figure 3(a-d) with concentrations (1 wt%) of Cu, Ni, and Co, exhibiting pseudo-capacitance behavior by anodic and cathodic peaks. The existence of a faradic current indicates behavior in metal oxide material [2-10]. Figure 3(a) shows the ZMO sample with an anodic (oxidation) peak at 0.45V, which is due to the Mn^{2+} to Mn^{3+} transition at a low scan rate of 5 mVs^{-1}. The cathodic reduction peaks present at 0.41 and 0.35V are due to the Mn^{3+} to Mn^{2+} and Zn^{2+} to Zn^{0} transitions, respectively. Figure 3(b) illustrates Cu-doped ZMO with 1 wt%, showing an oxidation peak around 0.45V due to Mn^{2+} to Mn^{3+} transition and enhanced by the presence of Cu^{2+} to Cu^{+} transitions. The two peaks in the reduction peak, the first peak being 0.40V, are attributed to the reduction of Mn^{2+} to Mn^{3+}. The second peak, which is 0.33V, is influenced by the presence of the Cu^{2+} to Cu^{+} transition [11]. Figure 3(c) shows the Ni-doped ZMO with 1 wt%, illustrating an oxidation peak at 0.42V, which is due to the Mn^{3+} to Mn^{4+} transition in the presence of Ni^{2+} to Ni^{+} transitions [4]. A reduction peak is noticed at 0.50V as a result of Mn^{4+} to Mn^{3+} transition at 5 mVs^{-1} scan rate and with a slight move to higher potentials as the scan rate rises to 100 mVs^{-1} in all CV. Figure 3(d) shows the Co-doped ZMO with a concentration of 1 wt%, which

exhibits an anodic peak at 0.42V due to the Mn^{2+} to Mn^{3+} transition. Furthermore, the presence of Co^{2+} to Co^{+} increases the potential to 0.46V. The cathodic peak observed at 0.34V is due to the Mn^{3+} to Mn^{2+} transition at a lower scan rate of 5 mVs^{-1} with a shift to higher potentials as the scan rate increases to 100 mVs^{-1} at 0.28V in all CV [7].

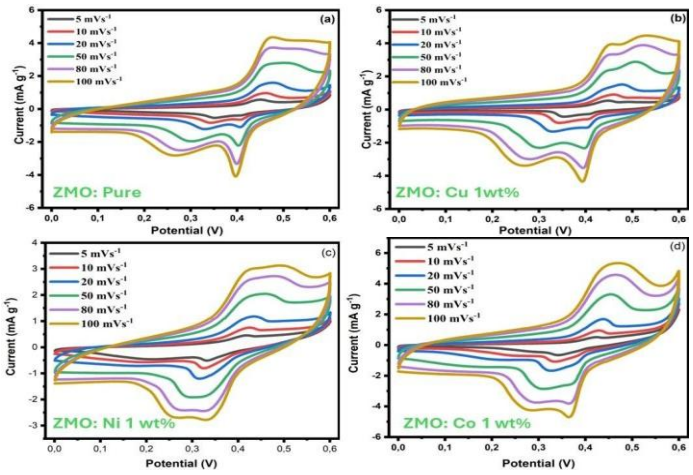

Figure 3: Shows CV curves of Co, Ni, and Cu $ZnMn_2O_4$ concentrations of (x = 0, 1 wt%) at varying scan rates.

The calculations for specific capacitance for the CV curves were computed using the following formula [11]

$$\text{Specific capacitance}(C_s) = \frac{\int I\mathrm{dv}}{s \times m \times \Delta V} \qquad (1)$$

where *I, S, V*, and *m* represent the current area in (mAs^{-1}), scan rate (mVs^{-1}), potential window (V), and the active mass (mg), respectively. The specific capacitance was calculated at varying scan rates of 5, 10, 20, 50, 80, and 100 mVs^{-1} for all samples. The calculated values are for Figure 3(a): 25.45, 18.97, 15.02, 10.80, 9.16, and 8.53 Fg^{-1}, respectively; In Figure 3(b), the specific capacitance calculations are 24.65, 17.78, 14.44, 11.37, 10.03, and 9.49 Fg^{-1}, respectively Figure 3(c): 31.37, 20.99, 14.70, 9.59, 7.89, and 7.26 Fg^{-1}, respectively. Additionally, Figure 3(d) shows the specific capacitance of ZMO: Co 1 wt% to be: 45.85, 29.47, 20.57, 14.03, 12.01, and 11.29 Fg^{-1}.

3.3.2 Galvanostatic charge-discharge (GCD)

The electrochemical performance for (GDD) is performed under a potential window of 0-0.6 V at various current densities of 3 to 5 Ag^{-1}. The three-electrode system was conducted in 2 M of potassium hydroxide (KOH) electrolyte, as shown in Figure 4(a-d). GCD curves show a symmetrical pattern for all current densities, indicating high coulombic efficiency. Moreover, the nonlinear charge/discharge profile further confirms a pseudocapacitive behavior of Co, Ni, and Cu-doped ZMO materials [7]. Figure 4(a) shows the GCD behavior of ZMO at various current densities, revealing that the charge and discharge processes take longer at lower current densities, which indicates that more charge is stored, suggesting that the material has a higher capacity at a lower current density. The discharge time also took longer, indicating that the material can release charge more slowly, which is favorable for battery-type applications requiring steady energy [10]. Figure 4(b) shows Cu-doped ZMO material with 1 wt% concentration, which exhibits an increase in charge and discharge time when compared to the ZMO material. Figure 4(c) shows the Ni-doped with a decrease in charge-discharge due to the potential window, which reduces conductivity. Figure 4(d) shows greater potential than other materials [12].

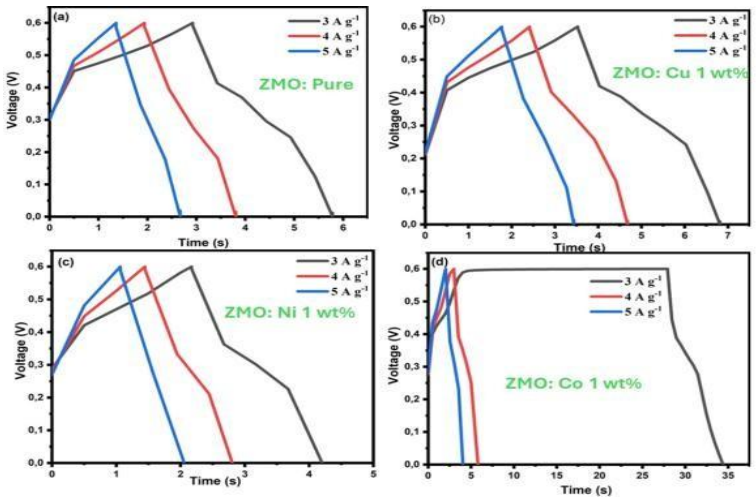

Figure 4:(a) Exhibit plots Galvanostatic charge-discharge of Co, Ni, and Cu-doped $ZnMn_2O_4$ at varying current densities.

The charge /discharge specific capacitance was computed using the following formula [9].

$$\text{Specific capacitance}(C_s) = \frac{\int Idt}{m\Delta V} \qquad (2)$$

where I, dt, m, ΔV represents the current area, change in discharge time, material mass, and potential window for the current densities of 3, 4, and 5 Ag^{-1}. The calculated specific capacitances for the ZMO sample are in Figure 5(a) 60.78, 48.03, 35.93 Fg^{-1}, (b)75.81, 63,89, 52.90 Fg^{-1}, (c) 41.87, (Ni)31.58, 23.55 Fg^{-1}, and (d) 686.88, 83.40, 75.15 Fg^{-1}

3.3.3 Electrochemical impedance spectroscopy (EIS)

Figure 5 shows the (EIS) spectrum, which was done to assess the electrochemical behavior of doped ZMO (x = 0, 1 wt%) of doped ZMO materials, measured within a frequency range of 10MHz – 100KHz in a potential window of 0-0.6V with an amplitude of 10 mV[12]. The Nyquist plots for the Cu, Ni, and Co concentrations were fitted using the equivalent electronic circuit as displayed in the Figure. The circuit is made up of R_1, which is an internal resistance (Rs), including the contact resistance of the current collector interfaces as well as the intrinsic resistance of the electrode and electrolyte. R_2 represents the charge transfer resistance (R_{ct}) observed in the low-frequency region, W_2 represents the Warburg resistance (Z_w), which is observed in low-frequency zone which is associated with electrode diffusion [11-12]. Cu-doped ZMO shows a steeper vertical line having the lowest resistance due to the smallest semicircle.

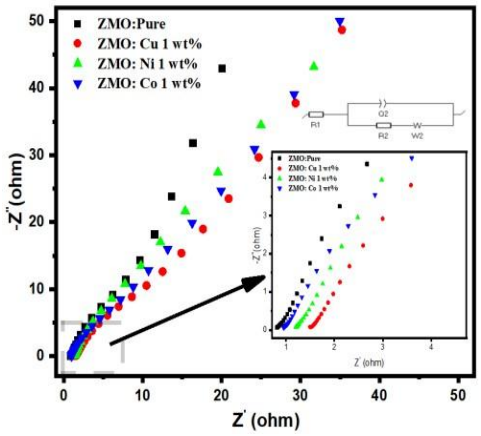

Figure 5: Nyquist plot of Co, Ni, and Cu-doped $ZnMn_2O_4$ with concentration of (x = 0 and 1 wt%).

4. Conclusion

The Co, Ni, and Cu-doped ZMO at a concentration of 1 wt% was successfully synthesized. XRD analysis shows a well-indexed single phase, with no impurities. Scanning Electron Microscopy (SEM) shows a similar morphology with nanoparticles that might enhance the conductivity of the material as concentrations are added. The electrochemical performance revealed that incorporating Co, Ni, and Cu into ZMO shows good stability, making it a great material for battery applications. C-V showing pseudo-capacitor behavior. The highest specific capacitance obtained for the ZMO: Co 1 wt% material was of the value, of 686.88 Fg^{-1}. This suggests that Co doped ZMO materials hold great potential for supercapacitor battery applications.

References

[1] Deva, P., S. Ravi, and C. Manoharan. "Synthesis of mesoporous structured $ZnMn_2O_4$ nanoparticles as an electrode for supercapacitor application." *Emergent Materials* (2024): 1-15.

[2] Kommu, P., Singh, G.P., Chakra, C.S., Jana, S., Kumar, V. and Bhattacharyya, A.S., 2020. Preparation of $ZnMn_2O_4$ and $ZnMn_2O_4$/graphene nano composites by combustion synthesis for their electrochemical properties. *Materials Science and Engineering*: B, 261, p.114647.

[3] Zhu, X., Wei, Z., Ma, L., Liang, J. and Zhang, X., 2020. Synthesis and electrochemical properties of Co-doped $ZnMn_2O_4$ hollow nanospheres. *Bulletin of Materials Science*, 43(1), p.4.

[4] Hasan, M., Zawar, S., Mustafa, G.M., Ghaffar, A., Razaq, A. and Atiq, S., 2022. Porous Architecture of Ni substituted $ZnMn_2O_4$ nanospheres as an electrode material for supercapacitor applications. *Physica B: Condensed Matter*, 633, p.413767.

[5] Aman, S., Ahmad, N., Manzoor, S., Alanazi, M.M., Abdelmohsen, S.A., Khosa, R.Y., Al-Sehemi, A.G., Hua, R., Alzahrani, H.A. and Chughtai, A.H., 2023. Effect of copper substitution on the electrocatalytic activity of $ZnMn_2O_4$ spinel embedded on reduced graphene oxide nanosheet for the oxygen evolution process. *Catalysis Surveys from Asia*, 27(2), pp.165-179.

[6] Sobhani, A. and Alinavaz, S., 2023. $ZnMn_2O_4$ nanostructures: synthesis via two different chemical methods, characterization, and photocatalytic applications for the degradation of new dyes. Heliyon, 9(11).

[7] Tao, Y., Li, Z., Tang, L., Pu, X., Cao, T., Cheng, D., Xu, Q., Liu, H., Wang, Y. and Xia, Y., 2020. Nickel and Cobalt Co-substituted spinel $ZnMn_2O_4$@ N-rGO for increased capacity and stability as a cathode material for rechargeable aqueous zinc-ion battery. *Electrochimica Acta*, 331, p.135296.

[8] Zhao, Y., Kumar, K.S., Ghanem, M.A., Roy, N., Kim, J.S. and Joo, S.W., 2024. In-situ synthesis of synergistic $ZnMn_2O_4$/MnOOH nanocomposite as a cutting-edge pseudocapacitive electrode material for all-solid-state asymmetric supercapacitors. *Ceramics International*, 50(23), pp.49834-49845

[9] Samage, A., Kuppe, P., Halakarni, M., Ganesan, B.K., Kamath, S.V., Yoon, H. and Kotrappanavar, N.S., 2024. Room temperature and rapid synthesis of $ZnMn_2O_4$ nanostructured spinel using deep eutectic solvent for high energy asymmetric supercapacitors. *Journal of Energy Storage*, 97, pp.112934.

[10] Ramesh, J.K., Rostami, S., Rajesh, J., Princess, R.M.B., Govindaraju, R., Kim, J., Adelung, R., Rajkumar, P. and Abdollahifar, M., 2025. $ZnMn_2O_4$ applications in batteries and supercapacitors: a comprehensive review. *Journal of Materials Chemistry A*, 13(20), pp.14540-14579.

[11] Wang, J., Shi, L., Wang, X. and Yang, L., 2025. Controllable preparation of flowered Cu-doped $Zn_{1-x}Cu_xMn_2O_4$ spinel and its application in electrode materials for supercapacitors. *Journal of Materials Science*: Materials in Electronics, 36(15), p.878.

[12] Saadi-motaallegh, S., Javanbakht, M., Omidvar, H. and Habibzadeh, S., 2023. A Novel Ni-doped $ZnMn_2O_4/Mn_2O_3$ nanocomposite synthesized by pulsed potential as superior zinc ion battery cathode material. *Journal of Alloys and Compounds*, *963*, p.171119.